JOURNAL OF COMPUTATIONAL PHYSICS 8, 268–284 (1971)

An Alternating Directional Implicit Scheme for Three-Dimensional Hypersonic Flows*

C. T. NARDO†

AND

R. J. CRESCI‡

Polytechnic Institute of Brooklyn, Preston R. Bassett Research Laboratory, Farmingdale, New York 11735

Received January 21, 1971

A theoretical and experimental investigation has been conducted of the behavior of steady low-density hypersonic flow over a finite-width flat plate.

The theoretical analysis, previously hampered by stability problems which dictated small streamwise increments, has been modified within the framework of the original formulation of Rudman and Rubin, in such a manner that larger streamwise increments are now possible without severe stability restrictions. This has been made possible by employing an alternating directional implicit numerical scheme developed by Peaceman and Rachford, such that the Rudman–Rubin analysis is now extendable downstream into the strong interaction region with smaller computational times.

Simultaneously, an experimental program was conducted to compare with the theoretical predictions. Measurements of pitot pressure and hot wire output (mass flow and temperature profiles) were obtained at two streamwise locations for several different plate widths. All tests were conducted for a Reynolds number of 300/inch and a temperature ratio ($\bar{T}_w/\bar{T}_{s_\infty}$) of 0.3. Profiles of density, velocity, and temperature ratios in the merged layer were obtained and compared to the theoretical analysis. Good agreement is shown to exist through the merged layer region.

* This research was supported by the Air Force Office of Scientific Research under Contract No. AF 49(638)-1623, Project No. 9781-01, under the technical supervision of Capt. W. H. Smith, USAF. This work is based upon a dissertation by the first author to the Polytechnic Institute of Brooklyn in partial fulfillment of the requirements for the degree of Doctor of Philosophy (Astronautics), June 1970.

† Formerly Post Doctoral Fellow; presently employed at Grumman Aerospace Corp., Propulsion Dept., Bethpage, New York 11714.

‡ Assistant Director of the Gas Dynamics Laboratory.

I. INTRODUCTION

Sustained flight at hypersonic velocities and extremely high altitudes is of significant current interest with respect to the space transportation system. The design and development of practical configurations in this flow regime is based on the ability to analyze and predict three-dimensional flow field effects. Heretofore, both experimental and analytical studies have concentrated mainly on two-dimensional or axisymmetric bodies in the rarefied flow regime, as typified by [1, 2], for example. In these references, one set of equations are postulated which are valid throughout the viscous-inviscid layer from the body surface to the free stream. As a result, a first order approximation to the full Navier–Stokes equations is obtained, resulting in a parabolic partial differential equation; this makes possible the use of finite-difference initial-value techniques to obtain the flow field description.

This approach is also adopted in the present study; however, an alternating directional implicit scheme is utilized in formulating the finite-difference equations for the three-dimensional flow. Previous investigations using explicit finite-difference techniques have been shown to be laborious for large core problems (such as a three-dimensional configuration) [3, 4] and, consequently, one might attempt to convert to a fully implicit technique. However, such a technique would require the solution of an (αM) by (αN) system of simultaneous algebraic equations at each streamwise step. Here, M and N represent the number of mesh points in each of the lateral directions (y and z) and α represents the number of independent variables. No recursion formulas are available for this type of technique and for large grid areas, iterative techniques are usually required. The alternating directional implicit technique is found to eliminate these difficulties. This technique requires the assumption of an initial solution at a given streamwise station. The conditions at the next station are obtained by representing y derivatives implicitly and z derivatives explicitly. In so doing, unknown variables are solved for simultaneously along lines of constant y. The solution at the next streamwise step is obtained by replacing y derivatives with an explicit formulation and z derivatives with an implicit scheme. This procedure continues downstream, alternately swtiching the implicit direction. This technique has been shown to be stable and convergent for linear, parabolic, second-order equations of the heat conduction type; however, the present analysis represents the first attempt to extend this numerical scheme to include a system of nonlinear, second-order partial differential equations in five unknowns. At present, it appears to be the most effective method for solving rectangular regions with a reduction in computational time of up to twenty-five times that of the identical explicit representation, and seven times over a Crank–Nicolson implicit scheme [4]. In addition, since one solves for one complete row or column at a time, a more tractable algorithm is produced.

This technique also permits a constant streamwise step size not subject to the stringent stability requirements of an explicit formulation, thereby allowing downstream integration at a much faster rate. As a result, three-dimensional flow-field calculations for configurations of practical interest, such as delta wings, waveriders, angle of attack effects, etc., can be readily obtained. With presently available computational schemes, these flow fields would require prohibitively long computing times.

The present study utilizes the finite-width flat-plate configuration for several reasons. First, an explicit analysis has been previously computed, and thus the relative efficacy of the two approaches can be compared. Second, this is a basic three-dimensional configuration which exhibits gradients in all coordinate directions, and can be modified to produce more practical flight configurations (e.g., altering the leading edge angle produces a typical delta wing).

II. Numerical Formulation of Equations

A detailed discussion of the reduction of the complete Navier–Stokes equations to the approximate form utilized in the present study is given in [1, 2, 5]. Briefly, however, Rudman and Rubin started with the governing Navier–Stokes equations nondimensionalized with respect to local reference values. They postulated that if the shock layer on a slender body is considered small, such that the normal gradients are much larger than either of the two lateral gradients (this ratio being denoted as δ^{-1}), one may write a first order approximation to the full Navier–Stokes equations. An exception occurred in the energy equation where δ^2 terms were retained in order to retain a nontrivial solution [1, 5]. Simultaneously, a second parameter $\Delta^2 = T_{\text{ref}}/\gamma M_\infty{}^2$ appeared in the expanded equations. Since T_{ref} represents the order of magnitude of the local temperature, one can easily show that $0.05 \leqslant \Delta^2 \leqslant 0.12$ depending upon the wall temperature (that is, cold or adiabatic wall) and, therefore, may also be considered small. Consequently, Δ^2 terms were also neglected which leads to the elimination of the streamwise pressure gradient. The consequences of this result are discussed in [1, 5]. Within this approximation, one can treat the x-momentum equations as a parabolic partial differential equation in which the inertia-viscous terms balance. The final equations for the steady, compressible viscous flow are repeated here for convenience:

Continuity:

$$(\rho u)_x + (\rho v)_y + (\rho w)_z = 0,$$

x-Momentum:

$$\rho u u_x + \rho v u_y + \rho w u_z = (\mu u_y)_y + (\mu u_z)_z ,$$

y-Momentum:

$$\rho u v_x + \rho v v_y + \rho w v_z = -p_y + \tfrac{4}{3}(\mu v_y)_y + (\mu u_y)_x - \tfrac{2}{3}(\mu u_x)_y - \tfrac{2}{3}(\mu w_z)_y + (\mu v_z)_z + (\mu w_y)_z ,$$

z-Momentum:

$$\rho u w_x + \rho v w_y + \rho w w_z = -p_z + \tfrac{4}{3}(\mu w_z)_z + (\mu w_y)_y + (\mu u_z)_x - \tfrac{2}{3}(\mu v_y)_z - \tfrac{2}{3}(\mu u_x)_z + (\mu v_z)_y ,$$

Energy:

$$\rho u T_x + \rho v T_y + \rho w T_z = -(\gamma - 1)\, p(u_x + v_y + w_z) + \frac{\gamma}{\sigma}(\mu T_y)_y + \frac{\gamma}{\sigma}(\mu T_z)_z + \gamma(\gamma - 1)\, M_\infty{}^2 \mu(u_y{}^2 + u_z{}^2) + \tfrac{4}{3}\mu(\gamma - 1)(v_y{}^2 + w_y{}^2 + w_z{}^2 - v_y w_z) + (\gamma - 1)\,\mu(w_y + v_z)^2,$$

State:

$$p = \rho T,$$

where p, ρ, T, and u are nondimensionalized with respect to their respective free stream values, μ with $\bar{\mu}_\infty M_\infty$, v and w with $\bar{u}_\infty \delta$, x with $\bar{L}$, and y and z with δ. Note that $\delta = \bar{\delta}/\bar{L} = (\gamma^{1/2} M_\infty)^{-1}$ and $\bar{L} = \gamma M_\infty{}^3(\bar{\mu}_\infty/\bar{\rho}_\infty \bar{u}_\infty)$. Also, dimensional quantities are barred ($^-$), whereas nondimensional quantities are unbarred ( ).

An alternating directional implicit finite difference scheme is now used to develop the difference equations corresponding to the above set of governing equations.

The methodology of the technique is as follows: first assume that the i, $i - 1$, $i - 2$,... planes are all known. It is desired to extend the solution downstream to the $i + 1$, $i + 2$,... planes. Using the coordinate system shown in Fig. 1, the i difference formulas are represented by a standard forward difference, namely,

$$\left(\frac{\partial \varphi}{\partial x}\right)_{j,k}^{i+1} = \frac{\varphi_{j,k}^{i+1} - \varphi_{j,k}^{i}}{\Delta x}$$

However, for planes in the direction of increasing x, this technique alternately takes y derivatives implicitly and z derivatives explicitly. That is,

$$\left(\frac{\partial \varphi}{\partial y}\right)_{j,k}^{i+1} = \frac{\varphi_{j+1,k}^{i+1} - \varphi_{j-1,k}^{i+1}}{2\Delta y} \qquad \text{(Implicit)}$$

and

$$\left(\frac{\partial \varphi}{\partial z}\right)_{j,k}^{i+1} = \frac{\varphi_{j,k+1}^{i} - \varphi_{j,k-1}^{i}}{2\Delta z} \qquad \text{(Explicit)}$$

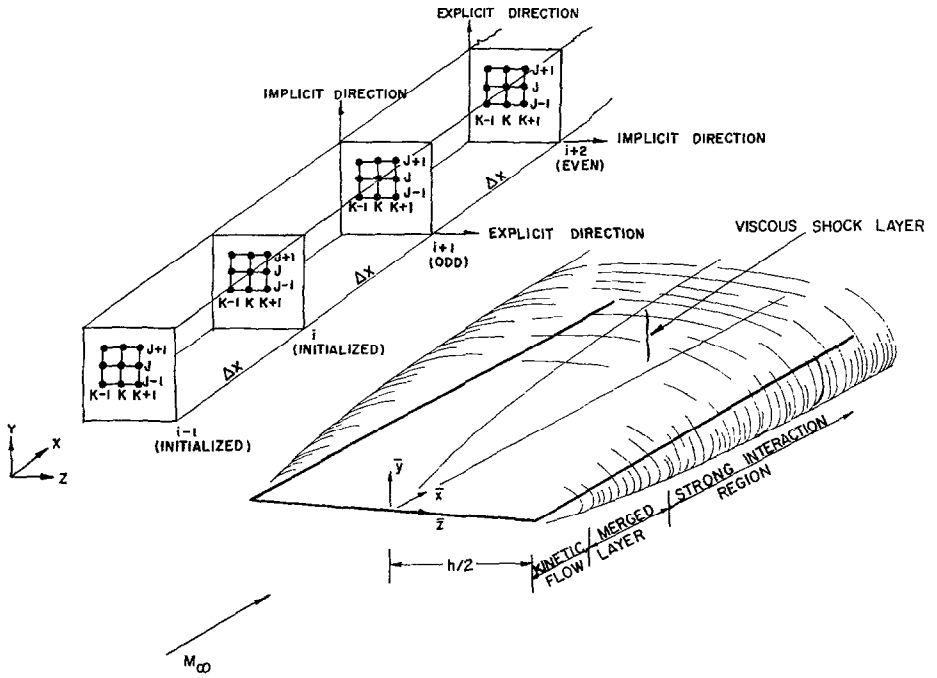

FIG. 1. Physical and numerical coordinate systems.

for the $i + 1$ plane. In the $i + 2$ plane, the difference equations for x remains the same; however, the y derivatives become explicit and the z derivatives implicit, namely,

$$\left(\frac{\partial \varphi}{\partial y}\right)_{j,k}^{i+2} = \frac{\varphi_{j+1,k}^{i+1} - \varphi_{j-1,k}^{i+1}}{2\Delta y} \qquad \text{(Explicit)}$$

and

$$\left(\frac{\partial \varphi}{\partial z}\right)_{j,k}^{i+2} = \frac{\varphi_{j,k+1}^{i+2} - \varphi_{j,k-1}^{i+2}}{2\Delta z}. \qquad \text{(Implicit)}$$

Thus, one complete row or column is solved at a time and hence only αM or αN simultaneous algebraic equations appear. Several items to be noted in the application of this technique are: (1) each streamwise increment x must remain constant for each advancement; (2) lateral increments, Δy and Δz, must remain equal to each other throughout the entire calculation since implicit and explicit directions are continually being interchanged; and (3) unilateral repitition in any one direction results in an unstable solution.

At present, this technique has been applied only to rectangular grids and its apparent success in comparison to other schemes has not been demonstrated for more general classes of equations and/or grid descriptions.

As an example of the type and form of the difference equations that are handled, the x-momentum equation for y implicit, z explicit is shown below:

$$\begin{aligned}
&\left\{\frac{\Delta\rho\,\Delta v}{2\Delta y} - \frac{\Delta\mu}{(\Delta y)^2} - \frac{\mu_4 - \mu_6}{4(\Delta y)^2}\right\} u_{j+1,k}^{i+1} + \left\{\frac{\Delta\rho\,\Delta u}{\Delta x} + \frac{2\Delta\mu}{(\Delta y)^2}\right\} u_{j,k}^{i+1} \\
&\quad + \left\{\frac{\mu_4 - \mu_6}{4(\Delta y)^2} - \frac{\Delta\mu}{(\Delta y)^2} - \frac{\Delta\rho\,\Delta v}{2\Delta y}\right\} u_{j-1,k}^{i+1} \\
&= \left\{\frac{\Delta\rho\,\Delta u}{\Delta x}\right\} u_5 + \left\{\frac{\mu_8 - \mu_{11}}{4(\Delta z)^2} - \frac{\Delta\rho\,\Delta w}{2\Delta z}\right\}(u_8 - u_{11}) \\
&\quad + \left\{\frac{\Delta\mu}{(\Delta z)^2}(u_8 - 2u_5 + u_{11})\right\},
\end{aligned}$$

where

$$\Delta(\ ) = 2(\ )_{j,k}^{i}(\ )_{j,k}^{i-1}$$

and subscripts

$$\begin{aligned}
4 &= i, j+1, k \\
5 &= i, j, k \\
6 &= i, j-1, k \\
8 &= i, j, k+1 \\
11 &= i, j, k-1.
\end{aligned}$$

Note the dependence of $u_{j,k}^{i+1}$ upon the values of u above and below it; this grouping of three mesh points per equation will be shown later to be advantageous.

Since there are five independent variables, five difference equations are required at each mesh point to describe adequately the flow field. For clarification, the following description of the algorithm used to solve the present problem was representative of the overall ADI technique used.

First, assume that the initial gridwork consists of five mesh points in each of the lateral directions, y and z, and that the first unknown plane, $i + 1$, is three, (planes 1 and 2 are known initial conditions). For $i + 1 = 3$, take y as the implicit direction. The calculation is started at $k = 2$ and the interior points, $j = 2, 3,$ and 4. For each of these three points, five difference equations can be written corresponding to the continuity, x-momentum, y-momentum, z-momentum, and energy equations. The five difference equations for $j = 2$ include unknown dependent variables at points 1 and 3. Similarly, the five difference equations for point 3 include unknowns at points 2 and 4 and so forth. These are the groupings of three mesh points that were referred to previously.

It is now necessary to specify the boundary conditions at points 1 and 5. Implicit difference equations are used such that a boundary equation at point 1 includes unknowns from points 2 and 3. The exact nature of the boundary condition used depends, of course, upon the geometry considered. Also, for the present configuration, a lateral gradient test was used to verify that the three-dimensional effects of the geometry had damped out.

One now has a collection of twenty-three difference equations for the five points of $k = 2$, both v_1 and v_5 being specified as zero, for purposes of this example. All twenty-three equations are linear and simultaneous, suggesting a matrix type solution to solve for the unknowns. It is here that the three mesh point dependency characteristics of the alternating directional implicit scheme became important. It can be shown that a band structure matrix can be formed by careful arrangement of the system of equations. This provides the possibility of utilizing an IBM scientific subroutine package denoted GELB which makes use of a Gaussian elimination technique to solve the system of equations. Not only does this subroutine decrease the amount of storage required by the program (by not dimensioning the two null corners of the matrix), but it also increases the program's overall speed and accuracy. The subroutine GELB solves a system of simultaneous linear algebraic equations by means of a Gaussian elimination technique that pivots the column elements only in order to preserve the band structure of the resulting coefficient matrices. In order to obtain initially a band structure, however, one must order the equations in the following manner:

y Implicit	*z Implicit*
1. y-momentum equation;	1. z-momentum equation;
2. x-momentum equation;	2. x-momentum equation;
3. energy equation;	3. energy equation;
4. z-momentum equation;	4. y-momentum equation;
5. continuity equation.	5. continuity equation.

In so doing, one can form the table shown in Fig. 2. This is a representative diagram for plane 3, k equal to 2 and JMAX equal to 5. Note that, since v_1 and v_5 (y-momentum equation) are both specified as zero, for the purposes of this example, they do not appear in the coefficient matrix. For this particular case, we have ten bands of elements above and nine bands below the principal diagonal and hence only need to dimension the elements in these bands. It is obvious that for large values of JMAX, the savings in storage space of this technique over

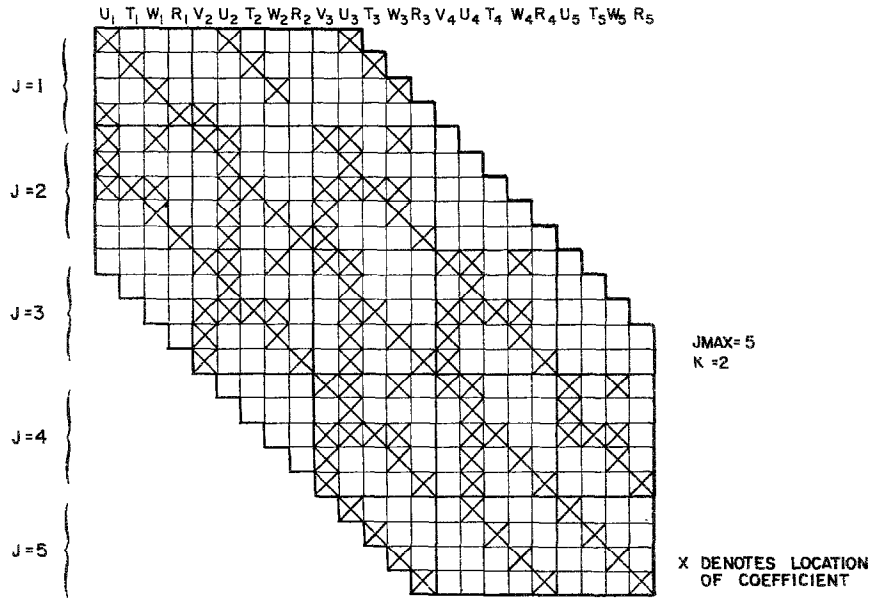

FIG. 2. GELB band structure chart.

another become sizeable. For example, if JMAX is equal to 50, the dimensions required for the coefficient matrix of GELB is 5153 whereas in a regular matrix inversion subroutine one would require 61,504 locations. Also, it is observed that for JMAX = 50, the order of the matrix is 5JMAX-2 or 248, and therefore, very large. It was found in some exploratory studies initially conducted to determine the most efficient and fastest method of solution of a system of difference equations, that GELB was three times as fast as a regular matrix inversion technique for a given tenth-order matrix. In addition, it was found that this speed factor was nonlinearly increasing in favor of GELB as the order of the matrix increased. This particular equation systematization, therefore, proved to be extremely beneficial.

The analysis is then reduced to the solution of large systems of linear algebraic

equations. The form of the boundary conditions and the specification of the initial conditions are discussed below so that the mathematical problem is completely posed.

The numerical scheme was then applied to the hypersonic, rarefied, viscous flow over a finite-width flat plate. This is a basic configuration upon which other more complicated three-dimensional geometries may be based. Accordingly, therefore, one may write the following set of boundary and initial conditions.

Boundary and Initial Conditions

Slip boundary conditions are enforced on the surface of the plate, namely,

ⓐ $y = 0;\ z \leqslant h/2;$

$$u = \lambda u_y\,; \quad w = \lambda w_y + 3(8\pi T)^{-1/2} T_z\,;$$

$$v = 0; \qquad T = T_w + \frac{2\gamma}{\gamma + 1}\left(\frac{\lambda}{\sigma}\right) T_y\,.$$

ⓐ $y = 0;\ z > h/2$:

u, w, T, ρ are symmetric;
v is antisymmetric

ⓐ $z = 0;\ y > 0$:

u, v, T, ρ are symmetric;
w is antisymmetric.

ⓐ $x = 0$:

freestream conditions are enforced;

and finally when

$(y^2 + z^2) \to \infty$:

$$\left.\begin{matrix} v \to 0 \\ w \to 0 \end{matrix}\right\} \quad \left.\begin{matrix} u \\ T \\ \rho \end{matrix}\right\} \to 1.$$

The rate at which the numerical solution converges toward the actual physical flow field depends to a degree upon the accuracy of the initial conditions and the streamwise step size.

One of the major objectives of this study was the determination of the effectiveness of an alternating directional implicit technique as a numerical tool in solving three-dimensional hypersonic-interaction problems. For this reason, initial calculations were duplications of earlier explicit runs to determine the speed and accuracy of the present technique. In particular, the Mach 25 case of [2] was rerun for comparison. A flat plate of 40 mean free paths in width was used to limit the large number of lateral grid points required to envelop adequately the disturbance region. The explicit calculation of [2] commenced at the centerline where symmetry conditions were enforced and then proceeded laterally and normally until the flow field parameters approached their freestream values to within a preset limit.

It took approximately forty minutes to reach $\bar{V} = 0.30$ which corresponds to three plate widths downstream of the leading edge. To test the accuracy of the

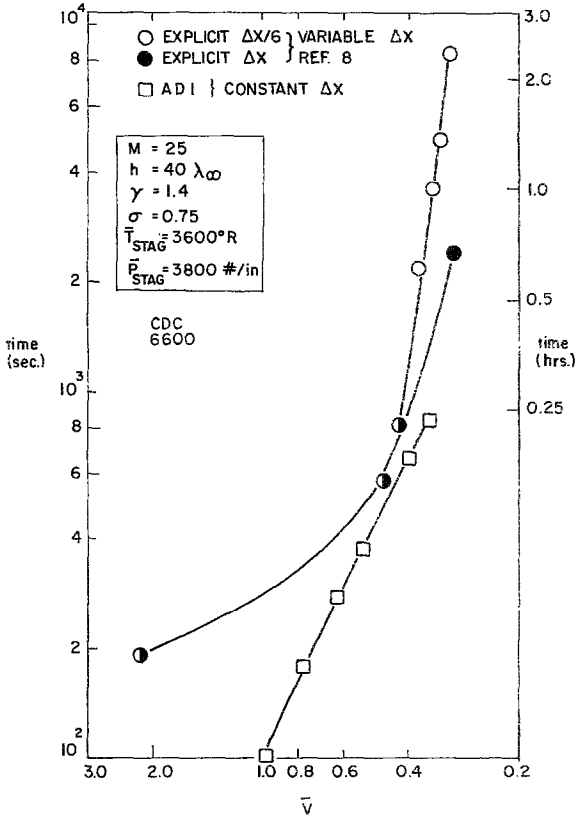

FIG. 3. Computational time comparison.

numerical result, the streamwise step size was then cut by a factor of six. It took almost two and one-half hours to then reach the same location. It was found that the difference in results between the two calculations varied by five to ten percent.

In applying the alternating directional implicit technique, only 15 minutes were necessary to reach $\bar{V} = 0.35$ (Fig. 3). This time saving was seen to increase as $\bar{V}$ decreased (or x increased). Moreover, the ADI technique was applied using a constant Δx. As the weak interaction regime was approached, the axial gradients

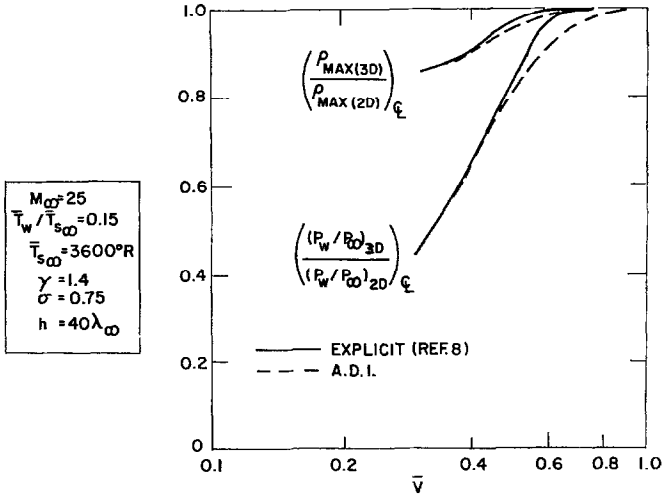

FIG. 4. Comparison of the centerline pressure and maximum density calculations.

decrease in strength and it is possible to increase Δx, thereby further decreasing the amount of time required to reach a given streamwise station; all times are referred to a CDC 6600. For a comparison of the accuracy of the ADI method and the explicit calculation, the centerline pressure and maximum density levels for both calculations are shown in Fig. 4 while the surface velocity is shown as a function of the lateral coordinate (at $\bar{V} = 0.35$) in Fig. 5. The centerline temperature profile for $\bar{V} = 0.35$ is also shown and compared to the explicit calculations. The results of the ADI calculation are seen to agree within approximately $3\frac{1}{2}$ percent with the explicit calculations for $\Delta x/6$, indicating that the ADI technique gives the same degree of accuracy in less computational time than the explicit scheme. The numerical solution to the governing equations was found to be highly dependent upon the initial conditions used for $\bar{V} \geqslant 0.45$. Therefore, no conclusions can be drawn from the analysis for higher values of $\bar{V}$, where it is observed that the two techniques yield different results.

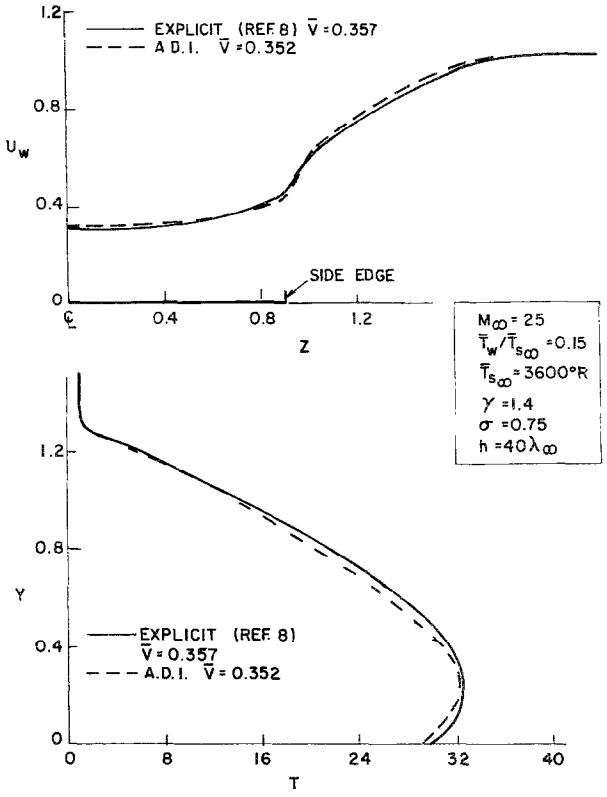

FIG. 5. Comparison of the slip velocity and centerline temperature profiles.

III. EXPERIMENTAL MEASUREMENTS

In order to evaluate the validity of the theoretical approach, an experimental program was initiated in which data was obtained and compared to the theoretical predictions. The flow environment was obtained in a unique fashion using a double nozzle blowdown tunnel; that is, a secondary nozzle placed in the test section of a larger blowdown tunnel. The double nozzle facility at the Polytechnic Institute of Brooklyn achieves a Mach number of 5.1 at a Reynolds number of 300/inch. For a two-inch model, this constitutes values of the rarefaction parameter ($\bar{V} = M_\infty/\sqrt{\mathrm{Re}_\infty}$) between ∞ and 0.2. It is interesting to note, in addition, that since the Mach number is so low, a sizeable strong interaction region never develops; instead the merged layer asymptotes into the weak interaction regime.

A two-dimensional flat plate model was investigated first in order to obtain

data for the "infinite" width plate. This model configuration was obtained by stretching a section of shimstock across the tunnel test section. In so doing, it was possible to eliminate the end effects.

The finite-width flat plates were made of the same 0.005″ shimstock material and were supported in a needle holder attached to a thicker sting. The tests were conducted on two plate widths, namely $1\frac{1}{2}$″ and 3/4″. On all plates, symmetry tests were run to ascertain any angle of attack effects which were found to be nonexistent within measurement accuracy.

The diagnostic tools used in determining the local flow conditions are pitot probes and the hot wire anemometer, which provided mass flow and temperature profiles, using the technique described in [6]. The details of the data acquisition and data reduction procedures, in addition to the complications and general problems of using hot wire anemometry in low density flow fields, are discussed at length in [7].

IV. Numerical and Experimental Results

The numerical analysis was then applied to the experimental test conditions for the present study. In Fig. 6, the predicted maximum density ratio along the centerline of the various width plates is presented as a function of $\bar{V}$. The two-dimensional theory of [1] is also shown. It is noted that data for the $h = 1\frac{1}{2}$ inch width plate is identical to the two-dimensional curve until a value of $\bar{V} = 0.40$ is achieved where the calculation was terminated. Thirty-four lateral points were required to specify this plate width and since additional points were required to envelop the complete disturbance region, the storage limitations of the computer were exceeded at $\bar{V} = 0.4$. It took approximately one hour to reach this station. Note that for these test conditions, (namely $M_\infty = 5.15$, $\mathrm{Re}_\infty/\mathrm{ft.} = 4.62 \times 10^3$) the effect of the initial conditions did not extend beyond $\bar{V} = .52$ as seen in Fig. 6.

Also shown are two additional calculations corresponding to finite plate widths of 3/4 inch and 3/8 inch. The 3/4 inch plate results are seen to coincide with the two-dimensional data until $\bar{V} = 0.45$. At this point, the peak density for the narrow plate starts to decrease below the two-dimensional value. The peak density for the smallest plate width investigated ($h = 3/8$″) was found to diverge from the two-dimensional curve very close to the leading edge; the three-dimensional lateral relief is significant even before the effects of the initial conditions have died out. The maximum density level for this configuration remains almost constant in the downstream direction, never reaching the Rankine–Hugoniot value. This calculation required fourteen minutes to reach $\bar{V} = 0.275$.

Of particular interest are the results presented in Fig. 7, where the surface pressure is shown as a function of lateral position normalized with respect to the

plate width. It is observed that the pressure level remains fairly constant over roughly 50% of the plate width. Even though the pressure is the most sensitive parameter associated with the lateral relief effect, the lateral pressure gradient is extremely small. It is noted, for example, for $h = 3/8''$ that the difference between the maximum and minimum values of the surface pressure is only 15%. However, the actual level of the centerline pressure is well below its two-dimensional counter-

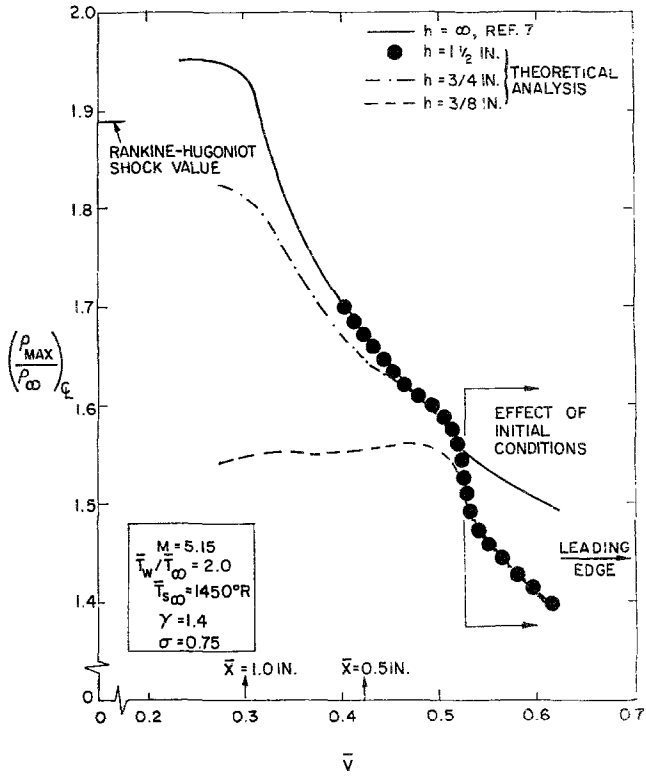

FIG. 6. Maximum centerline density variation for different plate widths.

part. It, therefore, becomes evident that the experimental investigation of two-dimensional models in merged layer flows must be carried out at very small values of $\bar{x}/h$ if truly two-dimensional values are to be obtained, since variations in the pressure level observed in the lateral direction are within the experimental accuracy of most test results. In Fig. 8, the maximum value of mass flow overshoot

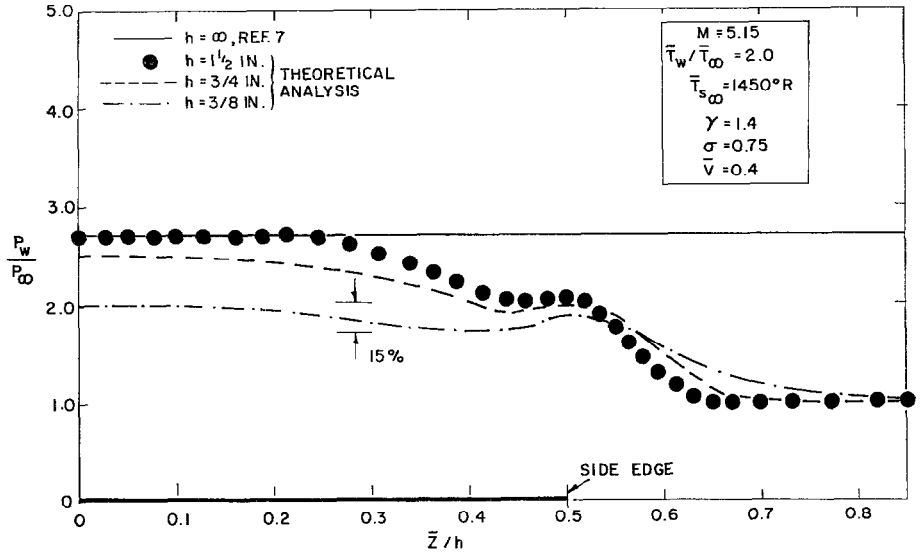

FIG. 7. Lateral surface pressure variation for different plate widths.

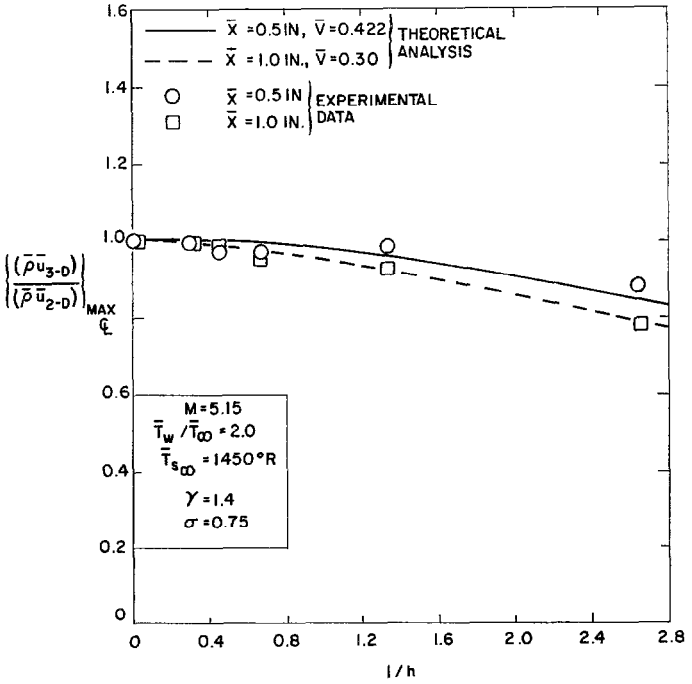

FIG. 8. Maximum centerline mass flow variation.

at the centerline of a finite width plate was normalized with respect to its counterpart in the two-dimensional case. In effect, the streamwise location is held constant and the plate width systematically decreased. It is obvious that $1/h$ is not the proper similarity parameter to use in the investigation of this type of lateral relief effect; the rarefaction parameter must also be considered. Also, the relief effect is more pronounced for the lower values of $\overline{V}$ at the same value of $1/h$, which one might expect intuitively. The data from the experimental program is also shown in Fig. 8 for comparison; the magnitude of the peak mass flow levels are seen to agree reasonably well with the theoretical results.

V. Concluding Remarks

A theoretical analysis and an experimental program has been conducted on the behavior of merged layer flow over a finite-width flat plate. A numerical scheme has been successfully applied using an alternating directional implicit (ADI) technique in which significant decreases in computational times are achieved in comparison to other current approaches. Experimental measurements have also been obtained and overall agreement between the theoretical results and the experimental data are quite good. The following conclusions are drawn:

(1) The alternating directional implicit scheme has significant utility in the numerical investigation of three-dimensional, hypersonic, viscous flow fields. Further study will be required, however, to refine the general approach and decrease computer storage requirements.

(2) The low density measurements obtained appear consistent with the theoretical predictions.

(3) Experimental, two-dimensional flow field investigations using finite width models must be performed with extreme care. The results presented herein indicate that the presence of small lateral gradients are not sufficient to insure two-dimensionality in merged layer flows.

References

1. S. Rudman and S. G. Rubin, *AIAA J.* **6**, 10, 1883–1889 (1968).
2. S. G. Rubin, T. C. Lin, M. Pierucci, and S. Rudman, *AIAA J.* 7, 9, 1744–1751 (1969).
3. R. J. Cresci, S. G. Rubin, C. T. Nardo and T. C. Lin, *AIAA J.* 7, 12, 2241–2246 (1969).
4. G. D. Smith, "Numerical Solution of Partial Differential Equations," Oxford University Press, London/New York, 1965.
5. H. K. Cheng, S. Y. Chen, R. Mobley, and C. R. Huber, The viscous hypersonic slender-body problem: a numerical approach based on a system of composite equations, Rand Corp., Memorandum RM-6139-PR, 1970.

6. E. M. SCHMIDT AND R. J. CRESCI, Hot wire anemometry in low density flows, Paper No. 70–589, AIAA 1970.
7. E. M. SCHMIDT, Ph.D. Thesis, Polytechnic Institute of Brooklyn, Brooklyn, New York, 1969.
8. C. T. NARDO AND R. J. CRESCI Merged layer flow over a finite width plate, paper presented at AIAA 3rd Fluid and Plasma Dynamics Conference, Los Angeles, Calif., June 29-July 1, 1970, Paper No. 70-784, AIAA.